Single-Molecule Tracking and Its Application in Biomolecular Binding Detection

Cong Liu, Yen-Liang Liu, Evan P. Perillo, Andrew K. Dunn, and Hsin-Chih Yeh

(Invited Paper)

***Abstract*—In the past two decades, significant advances have been made in single-molecule detection which enables the direct observation of single biomolecules at work in real time and under physiological conditions. In particular, the development of single-molecule tracking (SMT) microscopy allows us to monitor the motion paths of individual biomolecules in living systems, unveiling the localization dynamics, and transport modalities of the biomolecules that support the development of life. Beyond the capabilities of traditional camera-based tracking techniques, state-of-the-art SMT microscopies developed in recent years can record fluorescence lifetime while tracking a single molecule in the 3D space. This multiparameter detection capability can open the door to a wide range of investigations at the cellular or tissue level, including identification of molecular interaction hotspots and characterization of association/dissociation kinetics between molecules. In this review, we discuss various SMT techniques developed to date, with an emphasis on our recent development of the next generation 3D tracking system that not only achieves ultrahigh spatiotemporal resolution but also provides sufficient working depth suitable for live animal imaging. We also discuss the challenges that current SMT techniques are facing and the potential strategies to tackle those challenges.**

***Index Terms*—Single-molecule tracking, fluorescence imaging, fluorescence lifetime, FRET, TCSPC, TIRF, light-sheet microscopy, HILO, PSF engineering, maximum likelihood estimation.**

I. Introduction

SINGLE-molecule detection has revolutionized the way we study biological systems. It allows us to see stochastic processes or minor reaction pathways that would otherwise be masked in ensemble measurements [1]. The direct observation of individual biomolecules has shed light on the most fundamental molecular processes, including enzymatic turnovers [2], [3], gene regulation [4]–[7], translation [8]–[10], mRNA dynamics [11]–[13], protein folding [14], [15], ligand-receptor interaction [16], [17], and virus infection [18], [19]. In particular, single-molecule detection results have successfully unveiled intermediates during protein folding [20] and subpopulations of molecules in a mixture [21], which could not be observed by conventional ensemble measurement techniques.

The key to single-molecule detection lies in an extremely small detection volume. This is due to the fact that the signal-to-background ratio (SBR) is significantly improved when the detection volume is less than one femtoliter [1]. Two original techniques that provide small detection volumes for single-molecule detection are confocal and total-internal-reflection microscopy (TIRM). Having an effective detection volume about 0.2 femtoliter [22], confocal microscopy detects one molecule at a time as the molecule is flowing through or diffusing in-and-out of the detection volume in an aqueous solution, generating burst signals in the single-photon-counting devices. Such photon bursts can be analyzed for their intensity [23], spectrum [24], anisotropy [25], and fluorescence lifetime [26], thereby providing information on molecular size, conformation, and stoichiometry. However, as the average time for a diffusive molecule to traverse the detection volume of a confocal system is on the order of 1 ms, the resulting short burst signals cannot describe any underlying slow dynamic processes. Besides, the data throughput is low (one molecule at a time). On the other hand, TIRM offers a higher data throughput by employing a wide-field illumination scheme (thus hundreds of single molecules at the focal plane can be imaged at the same time). But due to the shallow penetration depth of evanescent wave field ($\sim$150 nm), single molecules have to be tethered to the surface for observation. Although the observation time of single molecules can be as long as minutes (only limited by photobleaching [27], [28]), immobilization is not a physiologically relevant condition. Perturbation caused by surface interaction can lead to artifacts in single-molecule measurements [15], [29]. TIRM is particularly useful for the cell-free, *in vitro* observation of single-molecule behaviors on surface. For instance, conformation change of enzymes [30] and Holiday junction structure dynamics [31] have been well characterized by TIRM at the single-molecule level.

Unlike the traditional single-molecule detection methods described above, single-molecule tracking (SMT), or single-particle tracking (SPT) techniques, allows researchers to follow the molecules of interest and record their motion paths. The 1st generation SMT methods are simply based on TIRM, with the additional capability to perform frame-by-frame video analysis. Single-molecule trajectories are plotted through the identification of the same single molecules in each frame and the calculation of displacements of these molecules in consecutive frames. While this frame-by-frame analysis can certainly reveal the 2D motion patterns of single molecules within the evanescent wave field [32]–[35], the 1st generation tracking methods can only investigate *in vitro* processes [36] or cellular processes on the membrane [37]. Besides, whenever the frame-by-frame analysis is used for trajectory analysis, the temporal resolution is defined by the camera's frame rate.

Manuscript received November 04, 2015; revised May 09, 2016; accepted May 10, 2016. Date of publication May 17, 2016; date of current version July 21, 2016. This work was supported by Texas 4000 Foundation and National Institutes of Health (1R21CA193038).

The authors are with the University of Texas at Austin, Austin, TX 78712 USA (e-mail: tim.yeh@austin.utexas.edu).

Color versions of one or more of the figures in this paper are available online at http://ieeexplore.ieee.org.

Digital Object Identifier 10.1109/JSTQE.2016.2568160

To be able to track hundreds of single molecules at a time in mammalian cells, a thin optical sectioning plane that can go tens of microns into specimens is required. Two methods to generate a thin optical sectioning plane are pseudo TIRM (HILO) [38] and light sheet microscopy [39], which we collectively term the 2nd generation SMT methods. Whereas the 2nd generation methods enable the investigation of single-molecule trajectories inside mammalian cells, they are still 2D tracking techniques. In other words, the 2nd generation methods require a time-consuming z-scan to observe molecular motion in the third dimension inside a mammalian cell [40].

To track single molecules directly in the 3D space without any optical scanning, the 3rd generation tracking methods have been proposed that can encode the z-position of the single molecules in their 2D images. The most straightforward way to do this is to create multiple imaging planes (using multiple cameras) and estimate the z-position based on the out-of-focus spot size at each imaging plane [41], [42]. Alternatively, the z-position can be encoded as the shape of the out-of-focus spot by taking advantage of astigmatism, where only one camera is needed [43]. The most notable effort in the development of 3rd generation tracking methods is the point-spread-function engineering, in which the single emitter no longer appears as a single round spot at the imaging plane. For instance, a single emitter can appear as two spots in the double-helix point-spread-function microscopy, in which the z-position of the emitter is derived from the orientation and the separation distance of the two resulting PSF spots [44].

From the 1st to the 3rd generation methods, the detection volume is either fixed or is passively scanned. If the molecules of interest diffuse far away from the detection volume, they are lost and their recorded trajectories terminate. In the 4th generation tracking methods, microscopes were designed to actively track a single emitter [45]. In fact Howard C. Berg first described a feedback-control system to track the motion of single bacteria in solution in 1971 [46]. The key idea behind feedback tracking is to employ an actuation mechanism that can keep the diffusing singe molecule in the center of the focused beam. This can be done by either constantly bringing the diffusing molecule back to the center of the focused laser beam (*i.e.* via moving the whole sample using a xyz piezo stage) or steering the laser beam to lock on the diffusing molecule. Trajectories of the tracked particles are thus plotted based on the motion history of the piezo stage or the galvo mirrors [45]. At first glance the 4th generation feedback tracking methods share similarities with the particle trapping methods (e.g. optical tweezers [47] and electrophoretic trap [48], [49]) in that they both try to keep the molecule of interest in the center of laser focus for long-term observation. But practically they are different techniques: in the 4th generation tracking methods the molecule of interest is free to diffuse in the 3D space, while in particle trapping methods the molecule is captured and spatially confined. As a result, optical traps cannot be used to monitor the native movements of single biomolecules inside live cells. In this review we call the 1st, 2nd and 3rd generation tracking microscopes the non-feedback SMT systems. We call the 4th generation tracking microscopes and later development the feedback SMT systems.

Although the non-feedback SMT microscopy shares similarities with single-molecule-based super-resolution microscopy [50] (PALM [51], STORM [52] and their variants [53], [54]) in design concepts and instrumentation, the non-feedback systems need additional efforts to establish correspondence between molecular images in consecutive frames [55]. Establishing unambiguous molecular correspondence is not straightforward and can be complicated by a number of factors (*e.g.* high molecular density and disappearance of molecules over time). Recently Saxton and others initiated the first community experiment comparing the performance of analysis methods for SPT data [56]. Whereas no single method performed best across all scenarios, the results revealed clear differences between the various approaches of which users of these tracking analysis methods should be aware [56]–[59].

One of the key differences between the non-feedback and the feedback tracking systems lies in that the feedback systems can be built based on single-pixel, single-photon-counting detectors, for instance APD (avalanche photodiode) and PMT (photomultiplier tubes), rather than cameras [60]–[62]. The use of single-pixel detectors for SMT not only drastically improves the temporal resolution but also allows additional information, for instance fluorescence lifetime, to be simultaneously acquired while tracking a particle [62], [63]. Although the capability to perform time-correlated single-photon counting (TCSPC) analysis while tracking the molecules can provide information beyond the motion paths of the tracked molecules, the data throughput of the feedback systems is low as only one molecule is actively tracked at a time.

While the 4th generation SMT systems are becoming a powerful research tool, all current methods suffered from one or more of the following problems: (1) difficult optical alignment due to the use of 4-5 single-pixel detectors [60], [61], (2) limited penetration depth due to the use of one-photon excitation [64], and (3) poor temporal resolution due to the use of camera [45] or laser scanning [65]. We recently developed a 5th generation SMT technique that solved the above issues associated with the 4th generation systems. Our method is called TSUNAMI – Tracking of Single particles Using Nonlinear And Multiplexed Illumination [62], which enables deep (up to 200 μm) and high-resolution 3D tracking of individual receptor complexes in a highly scattering multicellular environment. We believe TSUNAMI holds great promises for yielding new discoveries of molecular dynamics (*e.g.* receptor transport) in 3D tissues. A summary and comparison of the five generations of SMT systems is listed in Table I.

II. Non-Feedback SMT

As mentioned in the Introduction, the key to successful single-molecule detection lies in a sufficient SBR. Here background refers to out-of-focus fluorescence, fluorescent impurities, Rayleigh scattering (elastic scattering) and Raman scattering (inelastic scattering) [1]. An effective way to suppress the background is to use TIRM (the 1st generation SMT systems), where the decay length of evanescent wave generated by total internal reflection is about 150 nm. In other words, only the

TABLE I
OVERVIEW OF SMT TECHNIQUES

Generation	Design	Feature	References
1st	TIRM and image-based tracking, non-feedback	2D, only can track single molecules on cellular membranes or in *in-vitro* systems	[30], [31], [34], [66]–[68]
2nd	LSM and image-based tracking, non-feedback	Can track single molecules in mammalian cells, but requires a time-consuming z-scan to build 3D trajectories	[4], [39], [69]–[76]
3rd	3D, z-position encoded in the 2D image, non-feedback	Enable z-position characterization within the imaging depth of objective ($\sim \pm 1\ \mu$m)	[77]–[82]
4th	Feedback-control 3D tracking microscopy	Enable high-resolution 3D tracking and a large z-tracking range. Can measure fluorescence lifetime. Multiple detectors often required.	[60], [61], [64], [83]–[92]
5th	Feedback-control, multicolor and deep 3D tracking microscopy	Use one detector. Image depth up to 200 μm. Easy for multicolor detection.	[62], [93], [94]

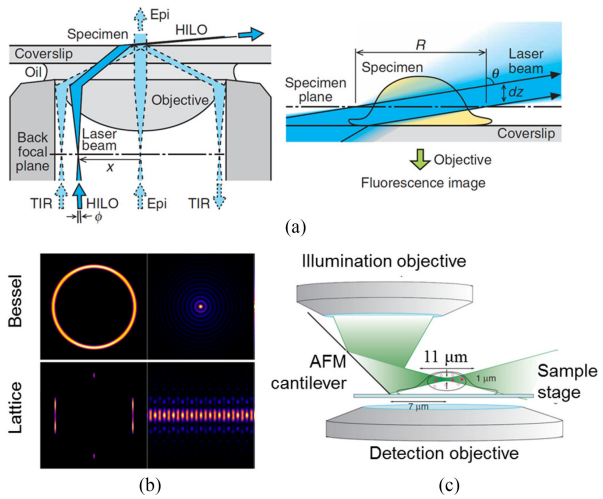

Fig. 1. Generation of thin illumination field (a) Highly inclined thin illumination optical sheet (HILO) microscopy. The incident beam is highly inclined and laminated as a thin light sheet in the specimen. TIR: total-internal-reflection fluorescence microscopy; Epi: epifluorescence. Reprinted by permission from Macmillan Publishers Ltd: Nature Methods [38], copyright 2008. (b) Bessel-beam and lattice light-sheeting microscopy. Left column: the intensity pattern at the rear pupil plane of the excitation objective. Right column: the cross-sectional intensity of the pattern in the xy plane at the focus of the excitation objective. From [102]. Reprinted with permission from AAAS. (c) Reflected light sheet microscopy (RLSM). A disposable mirror reflects the light sheet into a horizontal plane close to the sample surface. Because of the shape of the light sheet, a small gap between the surface and light sheet cannot be illuminated. Reprinted by permission from Macmillan Publishers Ltd: Nature Methods [106], copyright 2013.

molecules within this decay length can be illuminated and imaged. Microscopes equipped with high-N.A. (≥ 1.4) objectives are the most commonly adopted TIRM configuration which allows for easy switching between the TIRM and the standard epi-fluorescence imaging mode (Fig. 1(a) left). Whereas the shallow illumination depth of TIRM reduces background signals and also minimizes premature photobleaching, TIRM is not suitable for tracking molecules inside mammalian cells. Therefore, researchers mainly used TIRM for tracking molecules on cell membranes [16], [68], [95]–[97] or inside bacteria [98]. To bring intracellular molecules (*e.g.*, spliceosome in mammalian nucleus) into the evanescent field of TIRM, whole cell extract has been used [99]–[101].

To accommodate SMT inside mammalian cells, highly inclined thin illumination optical sheet (HILO) microscopy [38] and advanced light-sheet microscopy (LSM) [76], [102] were developed (the 2nd generation SMT systems). In HILO microscopy (Fig. 1(a)), the lateral position of the incident laser beam is somewhere in between the TIRM mode and the epi-fluorescence mode, allowing an inclined and laminated light sheet to penetrate into specimen [38]. The incident angle (ϕ) of the laser beam needs to be carefully adjusted in order to compensate the spherical aberration caused by the refractive index mismatch between the specimen and the coverslip [103], [104]. Besides, the reduction of the light-sheet thickness is accompanied by the decrease of the illumination area ($dz = R/\tan\theta$, Fig. 1(a) right panel). Moreover, HILO also suffers from fringing and shading artifacts [105]. Although out-of-focus fluorescence excitation due to the inclined nature of the illumination laser beam reduces SBR in detection [106], HILO microscopy has been used to track the active cargo transport along microtubules [72] and study surface dynamics of embryo with 200 nm-thick eggshell [74].

Other than HILO microscopy, advanced LSM provides an optical sectioning plane thin enough for SMT. The light sheet can be generated either by focusing the excitation laser one-dimensionally using a cylindrical lens [71], [75], [107]–[110], or by scanning a long Gaussian beam across a plane [69], [111]–[113]. In both schemes, there is a fundamental trade-off between the length and thickness of the light sheet due to the diffraction: the depth of focus ($2z_0$) of Gaussian beam (which decides the length of the light sheet) is directly proportional to the square of beam waist radius (W_0), $2z_0 = 2\pi W_0^2/\lambda_{\mathrm{exc}}$ [114], which decides the thickness of the light sheet.

To overcome this trade-off, Betzig's group turned to the Bessel-beam illumination and built Bessel-beam light sheet microscopy (Bessel LSM) [39], [76]. An ideal Bessel beam is diffraction free; it propagates indefinitely without change in cross-sectional intensity profile. In the implementation, a Bessel beam (actually a Bessel-Gaussian beam) is created by projecting an annular illumination pattern at the rear pupil of the excitation objective (Fig. 1(b)). The key advantage of the Bessel beam lies in that the thickness of the generated light sheet can be decoupled from the length of the light sheet. Consequently, the Bessel LSM provides a field of view as large as 50 μm $\times$ 50 μm with the illumination plane thickness as small as 500 nm, as compared to the 2–10 μm sheet thickness in the traditional Gaussian LSM [39]. Unfortunately, substantial energy of a Bessel beam resides in side lobes that surround the center peak, which excites the out-of-focus molecules and deteriorates the axial resolution.

A promising platform that eliminates the side-lobe issue and offers further gains in SBR is the lattice light sheet microscopy (lattice LSM) [102]. Optical lattice are periodic interference patterns (Fig. 1(b)) created by the coherent superposition of a finite number of plane waves. Like an ideal Bessel beam, an ideal 2D optical lattice is non-diffracting. In the implementation,

the 2D lattice is generated by a spatial light modulator that's conjugated to the back focal plane of the objective. The high-speed dithering of the lattice enabled by galvo mirrors creates a uniform light sheet. Without any side-lobe excitation, lattice LSM delivers a much lower peak intensity to the specimen than the conventional Gaussian/Bessel LSM (although total light dose delivered is similar), which is critical for cell health during the imaging [115]. The resolution of lattice LSM is comparable to that of a confocal microscope, but the recording speed and imaging duration are significantly improved [116].

One problem in LSM is the spatial constraints imposed by the two orthogonally arranged objectives—it is difficult to position the light sheet within 10 μm from the sample surface [106], making selective illumination of typical mammalian cell nuclei challenging. To overcome this limitation, reflected light sheet microscopy (RLSM) [106] and single-objective LSM [117] have been developed, which use a 45° micromirror or an atomic force microscopy cantilever to turn the vertical light sheet into the horizontal light sheet (Fig. 1(c)). Using RLSM, Xie's group has tracked individual transcription factor GR (glucocorticoid receptor) in MCF-7 cells and observed their binding to DNA in nuclei [106].

The superior optical sectioning capabilities of TIRM, HILO and advanced LSM make them ideal for 2D single-molecule imaging and tracking. However, without a z-scan these tools cannot provide information about the molecule's axial movement. Considering that most intracellular and some membrane-bound motions are inherently three dimensional [118], a true 3D SMT technique is highly desired.

One way to achieve 3D SMT is through multifocal plane imaging [42], [119]–[122]. Recently, a multifocus microscopy (MFM) that can produce an instant focal stack of nine images on a single camera has been reported [123]. In this scheme, a specially designed diffractive grating splits and shifts the focus of the sample emission light to form an instant focal series. Due to its fast 3D imaging capability, MFM has been used to study transcription dynamics [6], [13], gene editing [124] and other cell biology processes [125], [126].

An alternative approach is to encode molecule's z position in the microscope's 2D image. This can be done by an approach termed point-spread-function engineering (PSF engineering), where the PSF of the microscope is modified by using additional optical components (cylindrical lens, prism, spatial light modulator) in the detection path. After modification, the PSF is no longer symmetrical with respect to the focal plane [127] and the molecule's z position can be discerned from the asymmetric PSF with a position uncertainty even smaller than the diffraction limit of light [43].

There also exist other methods to resolve the molecule's z movement, including defocusing [128], [129] and interferometry [130]. As these approaches have limited applications in SMT inside live cells, they are not discussed in this review.

Astigmatism imaging is the simplest and perhaps the earliest example of PSF engineering for 3D SMT [77]. It is easy to implement and the working principle is applicable to various types of microscopy (*e.g.*, wide-field microscopy [119], [131], LSM [70], [132], and temporal focusing multiphoton excitation

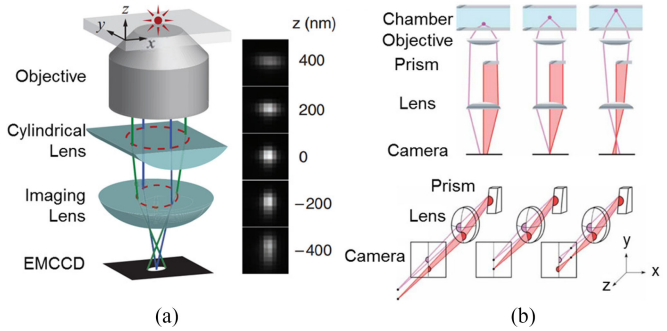

Fig. 2. Point-spread-function engineering without spatial light modulator. (a) Astigmatism imaging: a cylindrical lens is inserted into the imaging path to render the image of each molecule elliptical. The ellipticity and orientation of a fluorophore's image varied as its position changed in z. From [43]. Reprinted with permission from AAAS (b) 3D tracking using a prism: when the fluorescent molecule moves upward, the two beams of light split by the prism move symmetrically in opposite directions on the image. Reprinted by permission from Macmillan Publishers Ltd: Nature Structural and Molecular Biology [78], copyright 2008.

microscopy [133]). In astigmatism imaging, a weak cylindrical lens (another option is deformable mirror [134]) is inserted in the detection path, creating two slightly offset focal planes for the x and y directions in Fig. 2(a) [43]. As a result, images of fluorescent molecules are circular in the average focal plane (approximately halfway between the x and y focal planes) but ellipsoidal below or above the average focal plane. The centroid and ellipticity of the image are then used to determine the lateral (x and y) and axial (z) coordinates of the molecule respectively [135].

Another simple method to encode the z position in the fluorescent image is to place a wedge prism at the back focal plane of the objective (Fig. 2(b)) [78]. The fluorescence collected by the objective is split in two beams by the prism. The left half-beam (filled purple) passes through the center of the lens, whereas the right half-beam (filled red) refracted by the prism passes below the center. Thus molecule's z movement is converted to x movement at the image plane, where molecule's z position is reported by the x-separation of the two split images.

Comparing to cylindrical lens and prism, spatial light modulators (SLM) provide much more flexibility in PSF engineering and more control over the optical aberration which affects localization accuracy. A SLM is a liquid crystal based device that can modulate the phase, amplitude, or polarization of incident light as needed, but in SMT typically a phase-only SLM is used. Examples of PSF engineering using SLM for 3D SMT include double-helix PSF (DH-PSF) [79], [80], tetrapod PSF [81], self-bending PSF (SB-PSF) [82], corkscrew PSF [136], and bisected pupil PSF [137]. Due to their intrinsic similarity, only the first two techniques are discussed below.

The DH-PSF imaging system consists of a conventional inverted microscope and a 4*f* optical signal processing system as shown in Fig. 3(c). Specifically, the objective lens and tube lens form an image of the sample at an intermediate plane. The lens L1 placed at a distance *f* from this intermediate plane produces the Fourier transform of the image at a distance *f* behind the lens. The Fourier transform is then phased-modulated by

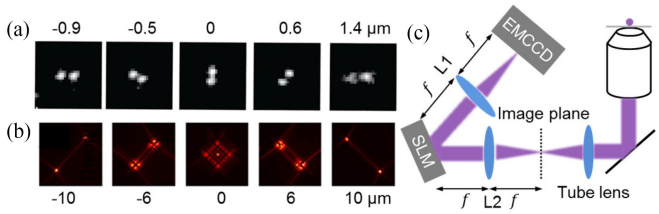

Fig. 3. Point-spread-function engineering with a spatial light modulator (SLM). (a) Images of a fluorescent bead at various axial positions in double-helix PSF imaging. Reprinted by permission from PNAS [44]. (b) Images of a fluorescent bead at various axial positions in tetrapod PSF imaging. (c) Optical path of the single-molecule double-helix or tetrapod PSF setup. Modified from PNAS [44].

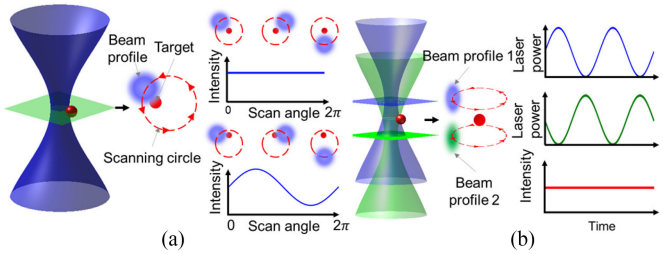

Fig. 4. Circularly scanning laser tracking (a) Lateral position sensing. The excitation laser scans circularly around the molecule. If the molecule is right at the center of the scanning circle, the fluorescence intensity remains constant during a scanning cycle (upper inset). If the molecule deviates a little from the center, the fluorescence intensity will exhibit modulation (lower inset). (b) Axial position sensing. Two laser beams rotating at the same frequency are focused at different depths inside the sample.

reflection from the LSM, and Fourier-transformed again by a second lens L2 (at a distance f to the SLM) onto the EMCCD to restore a real-space image [138]. As a consequence, a fluorescent molecule appears at the image plane as two lobs, and the two lobs have a unique orientation depending on the z-position of the molecule (Fig. 3(a)). The xy position of the molecule is estimated from the midpoint of the line connecting the two lobs, and z position is estimated from the angular orientation of the two lobs. Noticing that the failure to account for the molecule's transition dipole orientation can lead to significant lateral mislocalizations (up to 50–200 nm), the relative intensity of the two lobs is used as an additional parameter to determine the orientation of single-molecule emitter, which in turn can be utilized to correct the lateral localization [139].

In DH-PSF imaging, the depth over which one can determine the position of the molecules is only about 2 μm, posing a major limitation for applications requiring deep imaging and large-axial-range tracking. This limitation can be overcome by a tetrapod PSF design (Fig. 3(b)) which shares the same optical implementation with DH-PSF but provides an applicable z-range up to 20 μm. However, as PSF becomes more complex, the molecules in each image will need to be separated by greater distance for individual spots to be identified. Notably, Moerner's group has demonstrated a general method for PSF design that produces information-maximal PSF subject to system conditions (SBR, magnification and pixel size) [140]. Tetrapod PSF is just one solution to the optimization problem formulated in this work.

While engineered PSFs enable direct 3D tracking in the non-feedback systems, these 3rd generation tracking techniques require sophisticated calibration to accommodate factors that can distort the fluorescence images, such as emitter orientation, stage drift, the variation of localization accuracy across the field of view, and spherical aberration [79], [82], [139], [141]. It is this complication, as well as the difficulty in implementation (especially the phase modulation of fluorescence wavefront), that prevents the widespread use of the 3rd generation tracking methods at this moment. In fact, the conventional epi-fluorescence microscopy [142], [143], TIRM [36], [37], HILO [144] and LSM [102], [106] are the dominant techniques today to investigate the 3D cellular processes at the single-molecule level.

III. Feedback SMT

Feedback tracking systems have three major advantages over the non-feedback systems. First, the axial tracking range is no longer limited by the imaging depth of the objective (typically ± 1 μm), but rather by the travel range of piezo stage (± 50 μm). Second, there is no need for complicated PSF calibration as required in some 3rd generation tracking methods. Third, fluorescence lifetime of the tracer can be monitored simultaneously with its 3D position—thanks to the single-photon-counting detectors and TCSPC analysis.

One of the first 3D feedback SMT designs is the circularly scanning laser tracking (orbital tracking). To illustrate its working principle, here we assume that the molecule moves in a 2D plane. In this scheme, the laser beam is circularly scanning (enabled by acousto-optic modulators [64] or resonant beam deflectors [90]) at the frequency ω_{xy}. When the molecule is right at the center of the scanning circle (Fig. 4(a)), there's no signal intensity fluctuation during a scanning cycle. However, when the molecule deviates from the center, a sinusoidal variation of the signal over time can be observed. Therefore the molecule's lateral position can be derived from the magnitude and phase of this sinusoidal fluorescence signal [86]. To obtain the molecule's axial position in 3D tracking, two laser beams are required. They rotate at the same frequency ω_{xy} and are focused at different depths (separated by ~ 1 μm) inside the sample (Fig. 4(b)). More importantly, the optical powers in the beams are modulated 180° out-of-phase at the frequency ω_z (Fig. 4(b)), thus allowing the molecule's axial position to be encoded in the ω_z frequency component of the fluorescence signal. Once the molecule's 3D position is determined, a piezo stage is used to bring the molecule back to the center of scanning circle. Thus the stage position represent the single-molecule position over time.

The orbital tracking scheme works only when molecular motion is substantially small during each position estimation cycle (i.e. feedback bandwidth). To acquire the fast dynamic information (i.e. diffusion coefficient) of the molecule whose motion is comparable to the system bandwidth, fluorescence correlation analysis similar to the fluorescence correlation spectroscopy (FCS) can be performed [90]. However, the combination of SMT and FCS does not increase physical bandwidth, and the theory

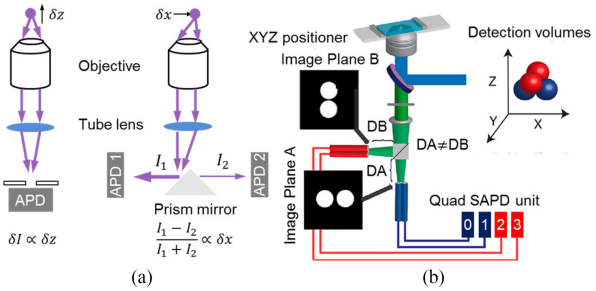

Fig. 5. (a) Confocal 3D tracking developed by Yang's group [148]. Part of the emission light collected by the objective lens is focused onto a pinhole. The intensity throughput provides a measure of molecular z position. To detect the molecular lateral position, the image of the molecule is projected onto the ridges of two orthogonal placed prism mirrors. Modified from [148]. (b) Confocal 3D tracking developed by Werner's group [83]. Two pairs of optical fibers are orthogonally installed. Each fiber is connected to an avalanche photodiode. The input face of each fiber serves as a pinhole, have a corresponding detection volume in the sample space (colored balls). One pair of fibers is axially separated from the other pair, so that the four detection volumes form a tetrahedron in the sample space. Modified from [83].

can only be applied to molecules undergoing isotropic Brownian diffusion. In other words, molecular motions such as active transport and sub-diffusion [145] are not accounted for using this hybrid analysis. Mabuchi's group has described a model of tracking error as a function of photon shot noise and molecule's diffusion coefficient [91], [146]. But again this model is only applicable to the free diffusion case. The original 3D orbital tracking system built by Gratton's group actually employed a two-photon excitation source, which gives a higher SBR and suppresses the out-of-focus photobleaching [88], [89]. Recently his group replaced the objective piezo with an electrically tunable lens, which provides not only a much longer axial tracking range (500 μm) but also a shorter step response time (2.5 ms) [147].

In the orbital tracking approach, the molecular position is encoded by modulating the spatial distribution of laser intensity, which takes place in the sample space. One can also encode the molecular position in the image space. This idea was first proposed by Howard C. Berg and implemented for tracking bacterial (scattering signal is detected) in 1971 [46]. But it wasn't until three decades later that tracking fluorescent nanoparticles or molecules became possible with this scheme, achieved separately by Yang's group [92], [148] and Werner's group [84], [85]. Their approaches are denoted as 3D confocal tracking here, since both of them utilized the spatial filtering effect typically seen in the confocal detection. In Yang's approach, a pinhole is placed at the focus of the tube lens, but slightly offset axially (Fig. 5(a) left). The fluorescence intensity through the pinhole will change as the molecule moves axially, thereby providing the z-position information. To detect the molecule's lateral position, the fluorescence emission is projected onto the ridges of two orthogonal prism mirrors, which split the signal to the two single-photon detectors (Fig. 5(a) right). When the molecule is centered, the detectors receive the same amount of photons. When the molecule moves laterally, the photon count difference between the detectors (normalized by the total photon count, termed error signals) will vary accordingly. The signals from the five detectors (one for z-position, two for x- and two for y-position) are fed to the controller, which sends a command to the xyz piezo-stage to bring the molecule back to the laser focus center for tracking. By combining the confocal tracking with the two-photon scanning microscopy, Yang's group has recently monitored cellular uptake of peptide-coated nanoparticles with a wide range of spatial and temporal resolutions [61].

Instead of using five detectors to achieve 3D confocal tracking, Werner's group used only four detectors. In Werner's approach (Fig. 5(b)), the emission is split into two beams, and each beam is focused onto the center of a custom-made fiber bundle that consists of two multimode optical fibers. Each fiber serves as a spatial filter for the APD (avalanche photodiode) connected to it. The two fiber bundles are orthogonally orientated and axially offset. The resulting detection volumes form a tetrahedral geometry in the sample space (Fig. 5(b) inset). A fluorescent molecule right in the center of the detection tetrahedron would give equal photon counts in the four detectors, but any displacement from the center would lead to asymmetric photon count distribution. This asymmetry, known as error signal, forms the basis for a feedback loop that drives the xyz piezo-stage to reposition the molecule to the center of the detection tetrahedron. Taking advantage of the single-photon detectors, Werner's group has demonstrated lifetime measurement [60], photon-pair correlation analysis (*i.e.* antibunching) [63] and time-gated detection [149] (beneficial for SMT in high background environment, *e.g.*, inside a cell) together with 3D SMT, which are not possible with camera-based tracking.

Confocal tracking has two advantages over orbital tracking. First, confocal tracking has a better SBR since the laser beam is locked directly on the molecule for tracking, rather than having a small offset from the molecule. Second, confocal tracking can achieve a higher temporal resolution because it does not require laser scanning to build up an intensity time trace for position estimation. Confocal tracking typically requires 4-5 single-photon counting devices to track single molecules in the 3D space. Recently our group demonstrated a 3D tracking microscope, termed TSUNAMI (Tracking of Single particles Using Nonlinear And Multiplexed Illumination), that only requires one PMT to achieve 3D SMT [62], [94]. The approach is based on passive pulse splitters used for nonlinear microscopy to achieve spatiotemporally multiplexed two-photon excitation and temporally demultiplexed detection to discern the 3D position of the molecule. In TSUNAMI, multiplexed illumination is realized by splitting the pulsed laser from a 76 MHz Ti-sapphire oscillator into four beams, with each beam delayed by 3.3 ns (one fourth of the laser repetition period) relative to its preceding one (Fig 6(a)). These beams are focused through a high N.A. objective at slightly offset xyz positions. The four resulting two-photon excitation volumes are arranged in a tetrahedral geometry, in a way similar to the detection volume arrangement in Werner's 3D confocal tracking system. In our case, the four excitation volumes receive laser pulses at different time frames. With TCSPC analysis, each detected photon is assigned to a 3.3 ns–wide time gate (G1-G4 in the fluorescence decay histogram (Figs. 6(b) and (c)), and thus can be attributed to a specific excitation volume. When the molecule sits right at the center of the excitation tetrahedron, the photon counts are approximately equal in

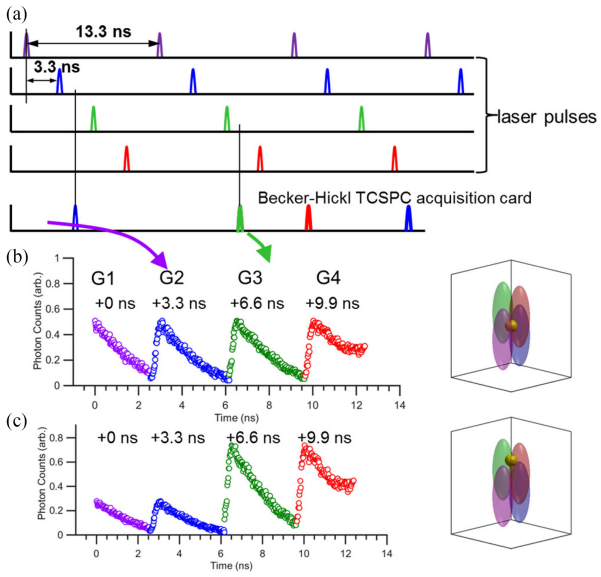

Fig. 6. Illustration of spatiotemporally multiplexed two-photon excitation and temporally demultiplexed detection (a) 76 MHz pulsed laser from a Ti-sapphire oscillator is split into 4 beams, with each beam delayed by 3.3 ns relative to the preceding one. (b) Using a TCSPC acquisition card, each detected photon can be assigned to a specific time gate (G1∼G4), leading to 4 fluorescence decay curves. The relative photon counts in each time gate (*i.e.* the area underneath the decay curve) can be used to infer the particle's 3D position. When the tracked particle is right at the center of the tetrahedron, photon counts in all time gates are about equal. The gold sphere in the excitation tetrahedron schematic represents the tracked particle. (c) When the particle moves away from the tetrahedron center, the photons counts in each time gate decrease or increase accordingly.

all four time gates. Any xyz displacement of the molecule from the center can be estimated *via* the normalized photon count difference in the four time gates (*i.e.* error signal). A closed feedback loop then drives the galvo mirrors and the objective z-piezo stage to lock the excitation tetrahedron on the molecule for tracking.

A two-photon microscope by nature, TSUNAMI enables multicolor imaging and imaging depth that cannot be achieved by the traditional one-photon feedback SMT microscopes. Our group has demonstrated 3D tracking of epidermal growth factor receptor complexes at a depth of ∼100 μm in live tumor spheroids [62]. At shallow depth, TSUNAMI has localization accuracy as good as 35 nm, and temporal resolution down to 50 μs (with bright fluorophores).

Despite the simplicity in implementation, it is worth noting that the error signal analysis used in the original TSUNAMI and confocal tracking microscopes is not optimal for molecular position estimation. Our recent work [93] demonstrated that a maximum likelihood estimator (MLE) (originally developed by Hell and Eggling for their non-feedback 2D confocal tracking microscope [150], [151]) can provide a much better axial position estimate without sacrificing lateral localization accuracy or temporal resolution. This MLE will be further discussed in the next section.

Orbital tracking, confocal tracking, and TSUNAMI microscopes are superior to the camera-based tracking systems in probing the fast dynamics of a single emitter. However, it can be equally important to find out how the single-molecule motion fits into the context of the entire biological system. This lack of contextual information (*e.g.*, cellular microdomains or neighboring molecules) poses the risk of misinterpreting the molecular behavior. Motivated by these concerns, Bewersdorf's group has developed a hybrid system that combines camera-based biplane imaging with feedback SMT [45], [152]. In Bewersdorf's design, fluorescence of the molecule is split and separately collected in the two regions of an EMCCD, whose conjugate planes in the sample space are axially offset by ∼750 nm. The fluorescence image acquired in either of these two regions directly reports the molecule's lateral position, whereas the image difference in the two regions can be used to discern the axial position. While using cameras for tracking could potentially facilitate co-registration of molecular trajectories and cellular images, camera-based tracking does not offer TCSPC analysis. It should be noted that spinning disk microscopy [149] and two-photon laser scanning microscopy [62] can easily be integrated into the orbital/confocal/TSUNAMI tracking microscopes to provide a view of slowly varying large-scale context where the rapidly diffusing molecules reside.

IV. Biomolecular Binding Detection Using Non-Feedback SMT

Biomolecular binding is one of the most fundamental processes in living systems. It plays critical roles in all corners of biology, such as DNA hybridization, membrane receptor signaling, and transcriptional regulation. Traditionally, molecular binding dynamics can be characterized by FRAP (fluorescence recovery after photobleaching) [153], [154], FCS [155], [156] and FCCS (fluorescence cross-correlation spectroscopy) [157]–[160]. Although FRAP, FCS and FCCS can achieve submillisecond temporal resolution in monitoring fast dynamic processes, the requirement of time-averaging of multiple events makes these traditional methods difficult in probing short-lived interactions and obtaining statistical properties from a heterogeneous sample [161]. On the other hand, with SMT, one can not only directly observe individual biomolecular binding events, but also recover transient intermediates [17], quantify equilibrium association and dissociation kinetics [34], [49], and characterize static and dynamic disorder [2].

Despite the recent advances in 3D SMT techniques, non-feedback 2D SMT (including wide-field, TIRF, and light sheet microscopy) is still the dominant approach for biomolecular binding detection at the single-molecule level. Instrument complexity could be one reason, but 3D feedback SMT has several more fundamental limitations. First, most 3D feedback SMT (orbital tracking, confocal tracking and TSUNAMI) systems track only one molecule at a time. To get sufficient tracking data for meaningful statistical analysis, a long measurement time is often required, indicating a low throughput at high cost. On the other hand, 2D SMT is beneficial for tracking multiple molecules simultaneously and probing interactions among them. Second, compared to the non-feedback 2D SMT microscopes, feedback microscopes often have a lower available photon budget (*i.e.* photon collection efficiency × total number of photons emitted by the molecule before photobleaching),

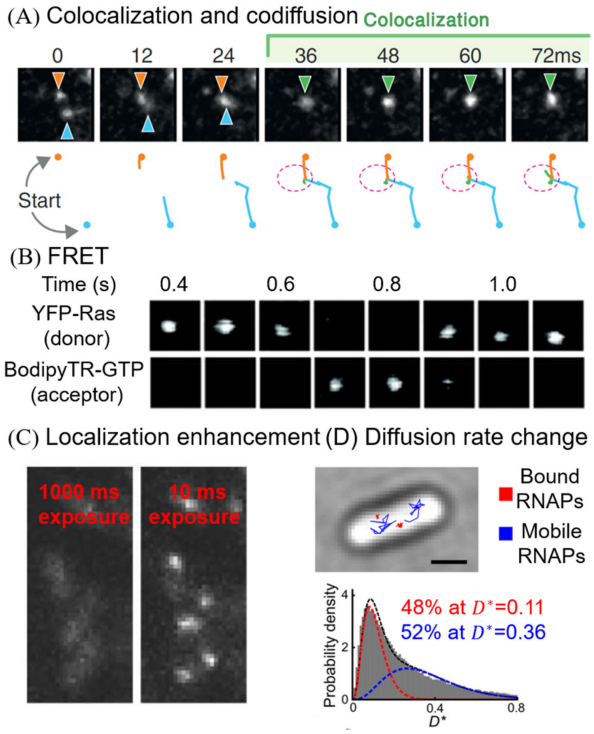

Fig. 7. Methods for biomolecular binding detection based on non-feedback 2D SMT microscopes. (a) Colocalization and codiffusion of binding partners. The image sequence shows two diffusing FPR (N-formyl peptide receptor, a class-A G-protein-coupled receptor) molecules and their trajectories. The two molecules first became colocalized (form FPR dimers) then diffuse together. Reprinted from [67]. (b) FRET Images of single YFP (donor) labeled small G-protein Ras and BodipyTR (acceptor) labeled GTP undergoing FRET upon Ras-GTP binding. Reprinted from [172]. (c) Localization enhancement. At 1000 ms, individual *lac* repressors (a transcription factor) appear as diffusive background. At 10 ms, they are visible as nearly diffraction-limited spots. The residence time of *lac* repressor on DNA is determined by obtaining fluorescence images at different exposure times. Reprinted from [4]. (D) Diffusion rate change. Individual RNAP (RNA polymerase) molecules are categorized as DNA-bound (example trajectories colored in red) or mobile (example trajectories colored in blue) based on their apparent diffusion coefficients D^*calculated from mean-squared-displacement (MSD) of their trajectories. The distribution of D^* can be fitted with two diffusing species (*i.e.* DNA-bound and mobile). Reprinted from [173].

resulting in fewer molecular position estimates. This is due to the fact that the confocal scheme used in the feedback systems has a much lower photon collection efficiency (0.5%–1%) as compared to that of the wide-field microscopy [162]. Although TSUNAMI provides a better collection efficiency by employing the non-descanned, single-detector scheme, two-photon excitation suffers from higher photobleaching rate as compared to one-photon excitation at comparable fluorescence emission rates [163], [164].

Four signatures of biomolecular binding events are usually measured by 2D SMT: colocalization/codiffusion, Förster resonance energy transfer (FRET), localization enhancement, and apparent diffusion rate change. Colocalization and codiffusion are the most commonly used signatures for binding detection at the single-molecule level [17], [34], [35], [165]–[167]. Using the dynamic dimerization of GPCR (G-protein-coupled receptor) [67] as an example (Fig. 7(a)): each GPCR monomer in the plasma membrane can be labeled with a fluorescent dye precisely at 1:1 ratio, and imaged as a bright spot on a TIRF microscope. Whether an observed spot represents a single GPCR monomer or a homodimer can be determined from its signal intensity level (or the number of bleaching steps [168]). In the time-lapse sequence of images, the dimerization of GPCR monomers would manifest itself as the colocalization and codiffusion of two monomer spots, whereas the splitting of one dimer spot into two monomer spots signals the opposite process. To detect the association of two different biomolecules, two-color single-molecule imaging can be performed in a similar way [16], [106], [169]–[171].

Since the molecular size is much smaller than the resolution (∼200 nm) of a TIRF microscope, incidental events where molecules reside within 200 nm from each other (called incidental colocalizations) can be misinterpreted as molecular binding. FRET, which occurs only when the donor and acceptor fall within ∼10 nm from each other [166], can be used to differentiate these two processes. As shown in Fig. 7(b), the binding of YFP-labeled Ras (donor) and BiodipyTR-labeled GTP (acceptor) is detected as the appearance of an emission spot of BiodipyTR-GTP colocalized with the YFP-Ras spot, and the appearance of BiodipyTR spot correlates with reduced YFP emission [172]. However, no FRET signal doesn't necessarily mean the absence of protein binding. The donor-acceptor pair and the labeling sites have to be carefully chosen for any FRET-based biomolecular binding studies.

The rest two signatures (localization enhancement and diffusion rate change) arise from the fact that biomolecular binding is usually accompanied by the slowdown of the molecule's diffusion. These signatures are often used in studying the association of transcription factor (TF) or RNA polymerase (RNAP) with chromatin DNA, where the TF/RNAP essentially becomes immobile upon DNA binding. Localization enhancement describes the phenomenon that when molecules are imaged with a camera using a long exposure time, fluorescence from the unbound molecules is collected over the entire field of view as these unbound molecules diffuse rapidly. On the other hand, bound molecules emit from a highly localized region, thus giving a signal higher than the autofluorescence background over time [4], [6]. By collecting fluorescence images at different exposure times, the residence time of TF/RNAP on chromatin DNA can be precisely determined (Fig. 7(c)). Compared with localization enhancement, direct analysis of the molecule's trajectory (*e.g.*, by mean-square-displacement calculation [174], cumulative probability distribution calculation [175], [176], hidden Markov modeling[177], and confinement analysis [178]) provides a more quantitative view of the molecular diffusion rate [102], [173] and residence time [6], [179] (Fig. 7(D)), which makes it suitable for studying binding processes that involves multiple molecular species and diffusive states [180].

V. Biomolecular Binding Detection Using Feedback SMT

As mentioned in Section III, feedback SMT microscopes are superior to non-feedback ones in several aspects. In particularly, the TSUNAMI microscope developed in our group is so

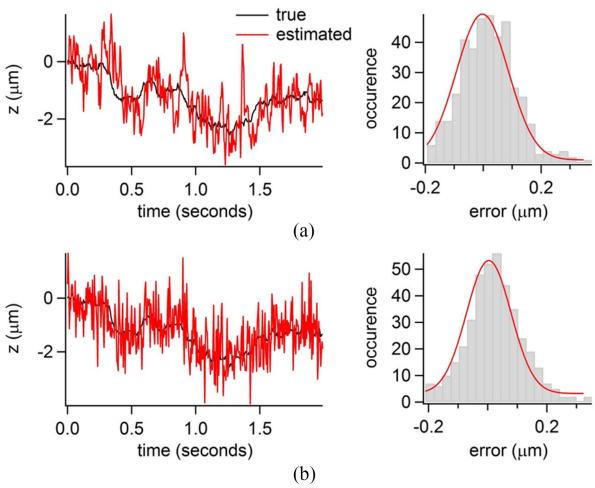

Fig. 8. Simulated z trajectories and the tracking error distribution. The red curves represent the estimated z trajectories while the black curves represent the true z trajectories of the diffusive particle. Tracking errors are exaggerated by 8× for easy visualization and comparison. In this simulation [93], the diffusive particle (D = 0.5 μm^2/s) is tracked for 2 seconds with TSUNAMI microscope. (a) There is persistent over-or under-estimation of z position within a time scale of ∼100 ms, indicating that the z-tracking error is temporally correlated. (b) The z-tracking error is white Gaussian tracking noise. It doesn't have any temporal correlation.

far the best choice for 3D biomolecular tracking in tissues, due to its large penetration depth, high SBR and great spatiotemporal resolution. However, our recent work [93] found that the current embodiment of TSUNAMI, as well as most other feedback tracking microscopes, has tracking error that is temporally correlated, which leads to questionable results in biomolecular binding kinetics measurements. In this section, we will elaborate the importance of temporally uncorrelated tracking error, and our approach to achieve that.

To observe the subtle change in diffusivity upon molecular associations or disassociations, it is critical to obtain a highly accurate molecule's 3D trajectory. The tracking error is a measure of the deviation of estimated molecular position from its true position, and it shouldn't be confused with the term "localization accuracy" used by the super-resolution imaging community [43], [181]–[184]. When studying the effects of tracking error on the molecular behavior interpretation, researchers often model the tracking error as time-independent white Gaussian noise [66], [174], [185]. While the white Gaussian noise model greatly simplifies mathematical analysis of localization error, the white Gaussian noise assumption may not be true in the real tracking experiments. Indeed, we have noticed that many of feedback tracking microscopes, including TSUNAMI, exhibit notable correlation in their tracking error [45], [61], [84], [85], [88], [146].

To illustrate the difference between white Gaussian error (WG error) and temporally correlated error (TC error), we plot the simulated z trajectories containing these two types of error in Fig. 8 [93]. The estimated trajectory (red curve) containing WG error (Fig. 8(b)) fluctuates rapidly over the true trajectory (black curve), while the estimated trajectory containing TC error shows persistent over- or under-estimation of the z position (Fig. 8(a)) within a time scale of ∼100 ms. To further quantify the degree of temporal correlation, the autocorrelation function [186] and power spectral density [187] of the tracking error are calculated [93]. Note that TC error and WG error are not differentiable from their histograms (Fig. 8), as both histograms show a nice Gaussian profile with similar mean and standard deviation. This is exactly why the temporal correlation property of tracking error has long been overlooked in the SMT community, as fitting a Gaussian curve to the tracking error histogram has been the only means to model the tracking error. Below we use DNA hybridization and melting kinetics as a model system to demonstrate that TC error can be detrimental for biomolecular binding kinetics characterization.

In the model system, the transition between the hybridized state (diffusion coefficient $\mathrm{D_h} = 0.15\ \mu\mathrm{m}^2\ /\mathrm{s}$) and the melted state ($\mathrm{D_m} = 0.30\ \mu\mathrm{m}^2\ /\mathrm{s}$) is a memoryless process, with a rate constant $k_{\mathrm{on}} = 2.99\times10^5\ \mathrm{M}^{-1}\mathrm{s}^{-1}$ for hybridization and a constant $k_{\mathrm{off}} = 0.7\ \mathrm{s}^{-1}$ for melting. The tracking duration is 1.5 s in our simulation, reflecting the photostability of a typical fluorescent tag. A hidden Markov model is adopted to model the random switch between the two diffusive states, and a 3D variational Bayes method (vbSPT) [180] is used to estimate the hybridization-melting kinetics (*i.e.* k_{on} and k_{off}) from the 3D trajectory data. Our simulations show that if the tracking error is temporally correlated, the relative error of estimated k_{on} and k_{off} can be as large as 29%; however, if the tracking errors are white Gaussian, the relative error is within ±4%. In our previous work (the same model system) [93], we have also shown that making the tracking error uncorrelated is as important as reducing the amplitude of tracking error (*i.e.* increasing spatial resolution).

The question then arises how tracking error can be decorrelated. Here is an intuitive thought: if the molecular position can be better determined in each feedback cycle (*e.g.*, through a more sophisticated analysis algorithm of the fluorescence signal), then consecutive over- or under- estimation of the molecular position over time should be reduced. Based on this thought, we have employed a MLE to estimate the molecule's 3D position, which can be readily applied to TSUNAMI and confocal tracking microscopes. The MLE algorithm takes the Poisson nature of photon counting into consideration, and treats the molecular position determination as a multivariate optimization problem (in contrast to the error signal analysis mentioned in Section III, where the x, y, and z positions are determined one by one) so that a global optimum can be reached. Our previous work [93] shows that MLE not only greatly decorrelates the tracking error, but also increases the z tracking accuracy of TSUNAMI microscope by 1.7 fold. By virtue of MLE, highly accurate molecular binding kinetics characterization based purely on molecular motion analysis has become possible.

Apart from molecular diffusivity, FRET signal is another signature of biomolecular binding that can be picked up by feedback SMT. FRET is particularly useful in the situation where molecular binding does not induce a significant change in diffusivity. Feedback SMT microscopes can easily perform lifetime-based FRET measurement, which doesn't require sophisticated calibration as needed by intensity-based FRET measurement used in non-feedback systems [188]. Since lifetime-based FRET

experiments only require the donor to be fluorescent, a dark quencher, instead of an organic dye, can be used as the acceptor. The challenge involved is that the quenching efficiency has to be carefully optimized. If the transfer efficiency is too high, the molecule in bound state would be very dim, making molecular tracking very difficult. On the other hand, if the efficiency is too low, no significant lifetime change would be observed upon molecular association/disassociation.

Here we have described five generations of the SMT microscopes. Currently there is no single solution that allows for super-resolution tracking of thousands of molecules in real time in live tissues. The next breakthroughs rely on advances in detector techniques, actuator techniques, objective techniques, laser and optical design.

REFERENCES

[1] C. Zander *et al.*, *Single Molecule Detection in Solution*. Hoboken, NJ, USA: Wiley, vol. 43, 2002.

[2] H. P. Lu *et al.*, "Single-molecule enzymatic dynamics," *Science*, vol. 282, pp. 1877–1882, 1998.

[3] A. M. van Oijen *et al.*, "Single-molecule kinetics of λ exonuclease reveal base dependence and dynamic disorder," *Science*, vol. 301, pp. 1235–1238, 2003.

[4] J. Elf *et al.*, "Probing transcription factor dynamics at the single-molecule level in a living cell," *Science*, vol. 316, pp. 1191–1194, 2007.

[5] D. Mazza *et al.*, "A benchmark for chromatin binding measurements in live cells," *Nucleic Acids Res*., p. gks701, 2012.

[6] J. Chen *et al.*, "Single-molecule dynamics of enhanceosome assembly in embryonic stem cells," *Cell*, vol. 156, pp. 1274–1285, 2014.

[7] F. Mueller *et al.*, "Quantifying transcription factor kinetics: At work or at play?" *Critical Rev. Biochem. Mol. Biol.*, vol. 48, pp. 492–514, 2013.

[8] L. Cai *et al.*, "Stochastic protein expression in individual cells at the single molecule level," *Nature*, vol. 440, pp. 358–362, 2006.

[9] B. Wu *et al.*, "Quantifying protein-mRNA interactions in single live cells," *Cell*, vol. 162, pp. 211–220, 2015.

[10] J. M. Halstead *et al.*, "An RNA biosensor for imaging the first round of translation from single cells to living animals," *Science*, vol. 347, pp. 1367–1671, 2015.

[11] Z. B. Katz *et al.*, "Mapping translation 'hot-spots' in live cells by tracking single molecules of mRNA and ribosomes," *Elife*, vol. 5, 2016, Art. no. e10415.

[12] N. Monnier *et al.*, "Inferring transient particle transport dynamics in live cells," *Nature Methods*, vol. 12, pp. 838–840, 2015.

[13] C. S. Smith *et al.*, "Nuclear accessibility of β-actin mRNA is measured by 3D single-molecule real-time tracking," *J. Cell Biol.*, vol. 209, pp. 609–619, 2015.

[14] H. S. Chung *et al.*, "Single-molecule fluorescence experiments determine protein folding transition path times," *Science*, vol. 335, pp. 981–984, 2012.

[15] H. S. Chung *et al.*, "Experimental determination of upper bound for transition path times in protein folding from single-molecule photon-by-photon trajectories," in *Proc. Nat. Acad. Sci. USA*, vol. 106, pp. 11837–11844, 2009.

[16] Y. Sako *et al.*, "Single-molecule imaging of EGFR signalling on the surface of living cells," *Nature Cell Biol*., vol. 2, pp. 168–172, 2000.

[17] Y. Teramura *et al.*, "Single-molecule analysis of epidermal growth factor binding on the surface of living cells," *The EMBO J*., vol. 25, pp. 4215–4222, 2006.

[18] S.-L. Liu *et al.*, "Effectively and efficiently dissecting the infection of influenza virus by quantum-dot-based single-particle tracking," *ACS Nano*, vol. 6, pp. 141–150, 2011.

[19] K.-I. Joo *et al.*, "Enhanced real-time monitoring of adeno-associated virus trafficking by virus–quantum dot conjugates," *ACS Nano*, vol. 5, pp. 3523–3535, 2011.

[20] E. A. Lipman *et al.*, "Single-molecule measurement of protein folding kinetics," *Science*, vol. 301, pp. 1233–1235, 2003.

[21] T. Ha *et al.*, "Single-molecule fluorescence spectroscopy of enzyme conformational dynamics and cleavage mechanism," in *Proc. Nat. Acad. Sci. USA*, vol. 96, pp. 893–898, 1999.

[22] T. A. Laurence and S. Weiss, "How to detect weak pairs," *Science*, vol. 299, pp. 667–668, 2003.

[23] A. N. Kapanidis *et al.*, "Fluorescence-aided molecule sorting: analysis of structure and interactions by alternating-laser excitation of single molecules," *Proc. Nat. Acad. Sci. USA*, vol. 101, pp. 8936–8941, 2004.

[24] M. Prummer *et al.*, "Single-molecule identification by spectrally and time-resolved fluorescence detection," *Anal. Chem.*, vol. 72, pp. 443–447, 2000.

[25] J. Schaffer *et al.*, "Identification of single molecules in aqueous solution by time-resolved fluorescence anisotropy," *J. Phys. Chem. A*, vol. 103, pp. 331–336, 1999.

[26] R. Müller *et al.*, "Time-resolved identification of single molecules in solution with a pulsed semiconductor diode laser," *Chem. Phys. lett.*, vol. 262, pp. 716–722, 1996.

[27] S. Myong *et al.*, "Repetitive shuttling of a motor protein on DNA," *Nature*, vol. 437, pp. 1321–1325, 2005.

[28] I. I. Cisse *et al.*, "A rule of seven in Watson-Crick base-pairing of mismatched sequences," *Nature Structural Mol. Biol.*, vol. 19, pp. 623–627, 2012.

[29] E. V. Kuzmenkina *et al.*, "Single-molecule Förster resonance energy transfer study of protein dynamics under denaturing conditions," *Proc. Nat. Acad. Sci. USA*, vol. 102, pp. 15471–15476, 2005.

[30] G. Luo *et al.*, "Single-molecule and ensemble fluorescence assays for a functionally important conformational change in T7 DNA polymerase," *Proc. Nat. Acad. Sci. USA*, vol. 104, pp. 12610–12615, 2007.

[31] S. A. McKinney *et al.*, "Structural dynamics of individual Holliday junctions," *Nature Structural Mol. Biol.*, vol. 10, pp. 93–97, 2003.

[32] A. Kusumi *et al.*, "Hierarchical organization of the plasma membrane: investigations by single-molecule tracking vs. fluorescence correlation spectroscopy," *Febs Lett*., vol. 584, pp. 1814–1823, 2010.

[33] A. Kusumi *et al.*, "Hierarchical mesoscale domain organization of the plasma membrane," *Trends Biochem. Sci.*, vol. 36, pp. 604–615, 2011.

[34] R. S. Kasai *et al.*, "Full characterization of GPCR monomer–dimer dynamic equilibrium by single molecule imaging," *J. Cell Biol.*, vol. 192, pp. 463–480, 2011.

[35] J. A. Hern *et al.*, "Formation and dissociation of M1 muscarinic receptor dimers seen by total internal reflection fluorescence imaging of single molecules," *Proc. Nat. Acad. Sci. USA*, vol. 107, pp. 2693–2698, 2010.

[36] A. Yildiz *et al.*, "Myosin V walks hand-over-hand: single fluorophore imaging with 1.5-nm localization," *Science*, vol. 300, pp. 2061–2065, 2003.

[37] A. R. Lowe *et al.*, "Selectivity mechanism of the nuclear pore complex characterized by single cargo tracking," *Nature*, vol. 467, pp. 600–603, Sep 2010.

[38] M. Tokunaga *et al.*, "Highly inclined thin illumination enables clear single-molecule imaging in cells," *Nature Methods*, vol. 5, pp. 159–161, Feb 2008.

[39] L. Gao *et al.*, "3D live fluorescence imaging of cellular dynamics using Bessel beam plane illumination microscopy," *Nature Protocols*, vol. 9, pp. 1083–1101, 2014.

[40] Z. Liu *et al.*, "3D imaging of Sox2 enhancer clusters in embryonic stem cells," *eLife*, vol. 3, 2014, Art. no. e04236.

[41] S. Ram *et al.*, "High accuracy 3D quantum dot tracking with multifocal plane microscopy for the study of fast intracellular dynamics in live cells," *Biophys. J.*, vol. 95, pp. 6025–6043, 2008.

[42] E. Toprak *et al.*, "Three-dimensional particle tracking via bifocal imaging," *Nano Lett*., vol. 7, pp. 2043–2045, 2007.

[43] B. Huang *et al.*, "Three-dimensional super-resolution imaging by stochastic optical reconstruction microscopy," *Science*, vol. 319, pp. 810–813, 2008.

[44] S. R. P. Pavani *et al.*, "Three-dimensional, single-molecule fluorescence imaging beyond the diffraction limit by using a double-helix point spread function," *Proc. Nat. Acad. Sci. USA*, vol. 106, pp. 2995–2999, 2009.

[45] M. F. Juette and J. Bewersdorf, "Three-dimensional tracking of single fluorescent particles with submillisecond temporal resolution," *Nano Lett*., vol. 10, pp. 4657–4663, 2010.

[46] H. C. Berg, "How to track bacteria," *Rev. Sci. Instrum.*, vol. 42, pp. 868–871, 1971.

[47] A. H. Yang *et al.*, "Optical manipulation of nanoparticles and biomolecules in sub-wavelength slot waveguides," *Nature*, vol. 457, pp. 71–75, 2009.

[48] A. E. Cohen and W. Moerner, "Suppressing Brownian motion of individual biomolecules in solution," *Proc. Nat. Acad. Sci. USA*, vol. 103, pp. 4362–4365, 2006.

[49] Q. Wang and W. Moerner, "Single-molecule motions enable direct visualization of biomolecular interactions in solution," *Nature Methods*, vol. 11, pp. 555–558, 2014.

[50] D. Toomre and J. Bewersdorf, "A new wave of cellular imaging," *Annu. Rev. Cell Developmental Biol.*, vol. 26, pp. 285–314, 2010.

[51] E. Betzig *et al.*, "Imaging intracellular fluorescent proteins at nanometer resolution," *Science*, vol. 313, pp. 1642–1645, 2006.

[52] M. J. Rust *et al.*, "Sub-diffraction-limit imaging by stochastic optical reconstruction microscopy (STORM)," *Nature Methods*, vol. 3, pp. 793–796, 2006.

[53] S. T. Hess *et al.*, "Ultra-high resolution imaging by fluorescence photoactivation localization microscopy," *Biophys. J.*, vol. 91, pp. 4258–4272, 2006.

[54] M. Heilemann *et al.*, "Subdiffraction-resolution fluorescence imaging with conventional fluorescent probes," *Angewandte Chemie Int. Ed.*, vol. 47, pp. 6172–6176, 2008.

[55] K. Jaqaman *et al.*, "Robust single-particle tracking in live-cell time-lapse sequences," *Nature Methods*, vol. 5, pp. 695–702, 2008.

[56] N. Chenouard *et al.*, "Objective comparison of particle tracking methods," *Nature Methods*, vol. 11, pp. 281–289, 2014.

[57] E. Meijering *et al.*, "Tracking in molecular bioimaging," *IEEE Signal Process. Mag.*, vol. 23, no. 3, pp. 46–53, May 2006.

[58] Y. Kalaidzidis, "Intracellular objects tracking," *Eur. J. Cell Biol.*, vol. 86, pp. 569–578, 2007.

[59] M. K. Cheezum *et al.*, "Quantitative comparison of algorithms for tracking single fluorescent particles," *Biophys. J.*, vol. 81, pp. 2378–2388, 2001.

[60] N. P. Wells *et al.*, "Time-resolved three-dimensional molecular tracking in live cells," *Nano Letters*, vol. 10, pp. 4732–4737, Nov. 2010.

[61] K. Welsher and H. Yang, "Multi-resolution 3D visualization of the early stages of cellular uptake of peptide-coated nanoparticles," *Nature Nanotechnol*., vol. 9, pp. 198–203, 2014.

[62] E. P. Perillo *et al.*, "Deep and high-resolution three-dimensional tracking of single particles using nonlinear and multiplexed illumination," *Nature Commun*., vol. 6, p. 7874, 2015.

[63] N. P. Wells *et al.*, "Confocal, three-dimensional tracking of individual quantum dots in high-background environments," *Anal. Chem.*, vol. 80, pp. 9830–9834, 2008.

[64] K. McHale *et al.*, "Quantum dot photon statistics measured by three-dimensional particle tracking," *Nano Lett*., vol. 7, pp. 3535–3539, 2007.

[65] V. Levi *et al.*, "3-D particle tracking in a two-photon microscope: application to the study of molecular dynamics in cells," *Biophys. J.*, vol. 88, pp. 2919–2928, 2005.

[66] C. Dietrich *et al.*, "Relationship of lipid rafts to transient confinement zones detected by single particle tracking," *Biophys. J.*, vol. 82, pp. 274–284, 2002.

[67] R. S. Kasai and A. Kusumi, "Single-molecule imaging revealed dynamic GPCR dimerization," *Curr. Opin. Cell Biol.*, vol. 27, pp. 78–86, 2014.

[68] A. Kusumi *et al.*, "Single-molecule tracking of membrane molecules: Plasma membrane compartmentalization and dynamic assembly of raft-philic signaling molecules," *Semin. Immunol.*, vol. 17, pp. 3–21, 2005.

[69] M. B. Ahrens *et al.*, "Whole-brain functional imaging at cellular resolution using light-sheet microscopy," *Nature Methods*, vol. 10, pp. 413–420, 2013.

[70] Y. Li *et al.*, "Light sheet microscopy for tracking single molecules on the apical surface of living cells," *J. Phys. Chem. B*, vol. 117, pp. 15503–15511, 2013.

[71] J. G. Ritter *et al.*, "Light sheet microscopy for single molecule tracking in living tissue," *PLoS One*, vol. 5, 2010, Art. no. e11639.

[72] K. Chen *et al.*, "Memoryless self-reinforcing directionality in endosomal active transport within living cells," *Nature Mater*., vol. 14, pp. 589–593, 2015.

[73] B. Wang *et al.*, "Bursts of active transport in living cells," *Phys. Rev. Lett.*, vol. 111, 2013, Art. no. 208102.

[74] F. B. Robin *et al.*, "Single-molecule analysis of cell surface dynamics in Caenorhabditis elegans embryos," *Nature Methods*, vol. 11, pp. 677–682, 2014.

[75] J. G. Ritter *et al.*, "High-contrast single-particle tracking by selective focal plane illumination microscopy," *Opt. Express*, vol. 16, pp. 7142–7152, 2008.

[76] T. A. Planchon *et al.*, "Rapid three-dimensional isotropic imaging of living cells using Bessel beam plane illumination," *Nature Methods*, vol. 8, pp. 417–423, 2011.

[77] H. P. Kao and A. Verkman, "Tracking of single fluorescent particles in three dimensions: use of cylindrical optics to encode particle position," *Biophys. J.*, vol. 67, 1994, Art no. 1291.

[78] J. Yajima *et al.*, "A torque component present in mitotic kinesin Eg5 revealed by three-dimensional tracking," *Nature Structural Mol. Biol.*, vol. 15, pp. 1119–1121, 2008.

[79] M. A. Thompson *et al.*, "Three-dimensional tracking of single mRNA particles in Saccharomyces cerevisiae using a double-helix point spread function," *Proc. Nat. Acad. Sci. USA*, vol. 107, pp. 17864–17871, 2010.

[80] A. Gahlmann *et al.*, "Quantitative multicolor subdiffraction imaging of bacterial protein ultrastructures in three dimensions," *Nano Lett*., vol. 13, pp. 987–993, 2013.

[81] Y. Shechtman *et al.*, "Precise 3D scan-free multiple-particle tracking over large axial ranges with Tetrapod point spread functions," *Nano Lett*., vol. 15, pp. 4194–4199, 2015.

[82] S. Jia *et al.*, "Isotropic three-dimensional super-resolution imaging with a self-bending point spread function," *Nature Photon*., vol. 8, pp. 302–306, 2014.

[83] J. J. Han *et al.*, "Time-resolved, confocal single-molecule tracking of individual organic dyes and fluorescent proteins in three dimensions," *ACS Nano*, vol. 6, pp. 8922–8932, 2012.

[84] G. A. Lessard *et al.*, "Three-dimensional tracking of individual quantum dots," *Appl. Phys. Lett.*, vol. 91, 2007, Art. no. 224106.

[85] G. A. Lessard *et al.*, "Three-dimensional tracking of fluorescent particles," *Biomed. Opt.*, vol. 2006, pp. 609205-1–609205-8, 2006.

[86] Y. Katayama *et al.*, "Real-time nanomicroscopy via three-dimensional single-particle tracking," *ChemPhysChem*, vol. 10, pp. 2458–2464, 2009.

[87] V. Levi and E. Gratton, "Three-dimensional particle tracking in a laser scanning fluorescence microscope," *Single Particle Tracking Single Mol. Energy Transfer*, pp. 1–24, 2009.

[88] V. Levi *et al.*, "3-D particle tracking in a two-photon microscope: application to the study of molecular dynamics in cells," *Biophys. J.*, vol. 88, pp. 2919–2928, 2005.

[89] V. Levi *et al.*, "Scanning FCS, a novel method for three-dimensional particle tracking," *Biochem. Soc. Trans.*, vol. 31, pp. 997–1000, 2003.

[90] A. Berglund and H. Mabuchi, "Tracking-FCS: Fluorescence correlation spectroscopy of individual particles," *Opt. Express*, vol. 13, pp. 8069–8082, 2005.

[91] A. J. Berglund *et al.*, "Feedback localization of freely diffusing fluorescent particles near the optical shot-noise limit," *Opt. Lett.*, vol. 32, pp. 145–147, 2007.

[92] C. S. Xu *et al.*, "Rapid and quantitative sizing of nanoparticles using three-dimensional single-particle tracking," *J. Phys. Chem. C*, vol. 111, pp. 32–35, 2007.

[93] C. Liu *et al.*, "Improving z-tracking accuracy in the two-photon single-particle tracking microscope," *Appl. Phys. Lett.*, vol. 107, 2015, Art no. 153701.

[94] E. Perillo *et al.*, "Single particle tracking through highly scattering media with multiplexed two-photon excitation," *Proc. SPIE*, vol. 9331, pp. 933107-1–933107-8, 2015.

[95] H. Ewers *et al.*, "Single-particle tracking of murine polyoma virus-like particles on live cells and artificial membranes," *Proc. Nat. Acad. Sci. USA*, vol. 102, pp. 15110–15115, 2005.

[96] M. Ott *et al.*, "Single-particle tracking reveals switching of the HIV fusion peptide between two diffusive modes in membranes," *J. Phys. Chem. B*, vol. 117, pp. 13308–13321, 2013.

[97] S. Manley *et al.*, "High-density mapping of single-molecule trajectories with photoactivated localization microscopy," *Nature Methods*, vol. 5, pp. 155–157, 2008.

[98] B. P. English *et al.*, "Single-molecule investigations of the stringent response machinery in living bacterial cells," *Proc. Nat. Acad. Sci. USA*, vol. 108, pp. E365–E373, 2011.

[99] I. Shcherbakova *et al.*, "Alternative spliceosome assembly pathways revealed by single-molecule fluorescence microscopy," *Cell Rep*., vol. 5, pp. 151–165, 2013.

[100] D. J. Crawford *et al.*, "Visualizing the splicing of single pre-mRNA molecules in whole cell extract," *RNA*, vol. 14, pp. 170–179, 2008.

[101] D. J. Crawford *et al.*, "Single-molecule colocalization FRET evidence that spliceosome activation precedes stable approach of 5′ splice site and branch site," *Proc. Nat. Acad. Sci. USA*, vol. 110, pp. 6783–6788, 2013.

[102] B.-C. Chen *et al.*, "Lattice light-sheet microscopy: Imaging molecules to embryos at high spatiotemporal resolution," *Science*, vol. 346, 2014, Art no. 1257998.

[103] B. Huang *et al.*, "Whole-cell 3D STORM reveals interactions between cellular structures with nanometer-scale resolution," *Nature Methods*, vol. 5, pp. 1047–1052, 2008.

[104] S. Liu *et al.*, "Three dimensional single molecule localization using a phase retrieved pupil function," *Opt. Express*, vol. 21, pp. 29462–29487, 2013.

[105] J. B. Bosse *et al.*, "Remodeling nuclear architecture allows efficient transport of herpesvirus capsids by diffusion," in *Proc. Nat. Acad. Sci. USA*, vol. 112, pp. E5725–E5733, 2015.

[106] J. C. M. Gebhardt *et al.*, "Single-molecule imaging of transcription factor binding to DNA in live mammalian cells," *Nature Methods*, vol. 10, pp. 421–426, 2013.

[107] J. Huisken *et al.*, "Optical sectioning deep inside live embryos by selective plane illumination microscopy," *Science*, vol. 305, pp. 1007–1009, 2004.

[108] K. Greger *et al.*, "Basic building units and properties of a fluorescence single plane illumination microscope," *Rev. Sci. Instrum.*, vol. 78, 2007, Art. no. 023705.

[109] F. C. Zanacchi *et al.*, "Live-cell 3D super-resolution imaging in thick biological samples," *Nature Methods*, vol. 8, pp. 1047–1049, 2011.

[110] M. Friedrich *et al.*, "Detection of single quantum dots in model organisms with sheet illumination microscopy," *Biochem. Biophys. Res. Commun.*, vol. 390, pp. 722–727, 2009.

[111] R. Tomer *et al.*, "Quantitative high-speed imaging of entire developing embryos with simultaneous multiview light-sheet microscopy," *Nature Methods*, vol. 9, pp. 755–763, 2012.

[112] P. J. Keller *et al.*, "Reconstruction of zebrafish early embryonic development by scanned light sheet microscopy," *Science*, vol. 322, pp. 1065–1069, 2008.

[113] P. J. Keller *et al.*, "Fast, high-contrast imaging of animal development with scanned light sheet-based structured-illumination microscopy," *Nature Methods*, vol. 7, pp. 637–642, 2010.

[114] B. E. Saleh *et al.*, *Fundamentals of Photonics*, vol. 22, New York, NY, USA: Wiley, 1991.

[115] R. Gräf *et al.*, "Live cell spinning disk microscopy," in *Microscopy Techniques*, New York, NY, USA: Springer, pp. 57–75, 2005.

[116] E. H. Stelzer, "Light-sheet fluorescence microscopy for quantitative biology," *Nature Methods*, vol. 12, pp. 23–26, 2015.

[117] R. Galland *et al.*, "3D high-and super-resolution imaging using single-objective SPIM," *Nature Methods*, vol. 12, pp. 641–644, 2015.

[118] N. P. Wells *et al.*, "Going beyond 2D: Following membrane diffusion and topography in the IgE-Fc [epsilon] RI system using 3-dimensional tracking microscopy," *Proc. SPIE*, vol. 7185, pp. 71850Z-1–71850Z-13, 2009.

[119] L. Holtzer *et al.*, "Nanometric three-dimensional tracking of individual quantum dots in cells," *Appl. Phys. Lett.*, vol. 90, 2007, Art. no. 053902.

[120] S. Ram *et al.*, "High accuracy 3D quantum dot tracking with multifocal plane microscopy for the study of fast intracellular dynamics in live cells," *Biophys. J.*, vol. 95, pp. 6025–6043, 2008.

[121] S. Ram *et al.*, "A novel approach to determining the three-dimensional location of microscopic objects with applications to 3D particle tracking," *Biomed. Opt.*, vol. 6443, pp. 64430D-1–64430D-7, 2007.

[122] P. Prabhat *et al.*, "Simultaneous imaging of different focal planes in fluorescence microscopy for the study of cellular dynamics in three dimensions," *IEEE Trans. NanoBiosci.*, vol. 3, no. 4, pp. 237–242, Dec. 2004.

[123] S. Abrahamsson *et al.*, "Fast multicolor 3D imaging using aberration-corrected multifocus microscopy," *Nature Methods*, vol. 10, pp. 60–63, 2013.

[124] S. C. Knight *et al.*, "Dynamics of CRISPR-Cas9 genome interrogation in living cells," *Science*, vol. 350, pp. 823–826, 2015.

[125] J. Wisniewski *et al.*, "Imaging the fate of histone Cse4 reveals de novo replacement in S phase and subsequent stable residence at centromeres," *Elife*, vol. 3, 2014, Art. no. e02203.

[126] B. Hajj *et al.*, "Whole-cell, multicolor superresolution imaging using volumetric multifocus microscopy," *Proc. Nat. Acad. Sci. USA*, vol. 111, pp. 17480–17485, 2014.

[127] S. W. Hell *et al.*, "Enhancing the axial resolution in far-field light microscopy: Two-photon 4Pi confocal fluorescence microscopy," *J. Modern Phys.*, vol. 41, pp. 675–681, 1994.

[128] A. Van Oijen *et al.*, "3-Dimensional super-resolution by spectrally selective imaging," *Chem. Phys. lett.*, vol. 292, pp. 183–187, 1998.

[129] M. Speidel *et al.*, "Three-dimensional tracking of fluorescent nanoparticles with subnanometer precision by use of off-focus imaging," *Opt. Lett.*, vol. 28, pp. 69–71, 2003.

[130] G. Shtengel *et al.*, "Interferometric fluorescent super-resolution microscopy resolves 3D cellular ultrastructure," *Proc. Nat. Acad. Sci. USA*, vol. 106, pp. 3125–3130, 2009.

[131] S. Ito *et al.*, "Restricted diffusion of guest molecules in polymer thin films on solid substrates as revealed by three-dimensional single-molecule tracking," *Chem. Commun.*, vol. 51, pp. 13756–13759, 2015.

[132] J.-H. Spille *et al.*, "Direct observation of mobility state transitions in RNA trajectories by sensitive single molecule feedback tracking," *Nucleic Acids Res.*, vol. 43, 2014, Art. no. e14.

[133] C.-H. Lien *et al.*, "Dynamic particle tracking via temporal focusing multiphoton microscopy with astigmatism imaging," *Opt. Express*, vol. 22, pp. 27290–27299, 2014.

[134] I. Izeddin *et al.*, "PSF shaping using adaptive optics for three-dimensional single-molecule super-resolution imaging and tracking," *Opt. Express*, vol. 20, pp. 4957–4967, 2012.

[135] S. A. Jones *et al.*, "Fast, three-dimensional super-resolution imaging of live cells," *Nature Methods*, vol. 8, pp. 499–505, 2011.

[136] M. D. Lew *et al.*, "Corkscrew point spread function for far-field three-dimensional nanoscale localization of pointlike objects," *Opt. Lett.*, vol. 36, pp. 202–204, 2011.

[137] A. S. Backer *et al.*, "A bisected pupil for studying single-molecule orientational dynamics and its application to three-dimensional super-resolution microscopy," *Appl. Phys. Lett.*, vol. 104, 2014, Art no. 193701.

[138] M. A. Thompson *et al.*, "Localizing and tracking single nanoscale emitters in three dimensions with high spatiotemporal resolution using a double-helix point spread function," *Nano Lett.*, vol. 10, pp. 211–218, 2009.

[139] M. P. Backlund *et al.*, "Simultaneous, accurate measurement of the 3D position and orientation of single molecules," *Proc. Nat. Acad. Sci. USA*, vol. 109, pp. 19087–19092, 2012.

[140] Y. Shechtman *et al.*, "Optimal point spread function design for 3D imaging," *Phys. Rev. Lett.*, vol. 113, 2014, Art. no. 133902.

[141] S. Ghosh and C. Preza, "Characterization of a three-dimensional double-helix point-spread function for fluorescence microscopy in the presence of spherical aberration," *J. Biomed. Opt.*, vol. 18, pp. 036010–036010, 2013.

[142] M. Lakadamyali *et al.*, "Visualizing infection of individual influenza viruses," *Proc. Nat. Acad. Sci. USA*, vol. 100, pp. 9280–9285, 2003.

[143] S. Courty *et al.*, "Tracking individual kinesin motors in living cells using single quantum-dot imaging," *Nano Lett.*, vol. 6, pp. 1491–1495, 2006.

[144] I. Izeddin *et al.*, "Single-molecule tracking in live cells reveals distinct target-search strategies of transcription factors in the nucleus," *Elife*, vol. 3, 2014, Art. no. e02230.

[145] M. J. Saxton and K. Jacobson, "Single-particle tracking: applications to membrane dynamics," *Annu. Rev. Biophys. Biomol. Structure*, vol. 26, pp. 373–399, 1997.

[146] A. J. Berglund and H. Mabuchi, "Performance bounds on single-particle tracking by fluorescence modulation," *Appl. Phys. B*, vol. 83, pp. 127–133, 2006.

[147] P. Annibale *et al.*, "Electrically tunable lens speeds up 3D orbital tracking," *Biomed. Opt. Express*, vol. 6, pp. 2181–2190, 2015.

[148] H. Cang *et al.*, "Guiding a confocal microscope by single fluorescent nanoparticles," *Opt. Lett.*, vol. 32, pp. 2729–2731, 2007.

[149] M. S. DeVore *et al.*, "Three dimensional time-gated tracking of non-blinking quantum dots in live cells," *Proc. SPIE*, vol. 12, pp. 933812-1–933812-15, 2015.

[150] S. J. Sahl *et al.*, "Fast molecular tracking maps nanoscale dynamics of plasma membrane lipids," *Proc. Nat. Acad. Sci. USA*, vol. 107, pp. 6829–6834, 2010.

[151] S. J. Sahl *et al.*, "High-Resolution tracking of single-Molecule diffusion in membranes by confocalized and spatially differentiated fluorescence photon stream recording," *ChemPhysChem*, vol. 15, pp. 771–783, 2014.

[152] M. F. Juette *et al.*, "Three-dimensional sub–100 nm resolution fluorescence microscopy of thick samples," *Nature Methods*, vol. 5, pp. 527–529, 2008.

[153] B. L. Sprague and J. G. McNally, "FRAP analysis of binding: Proper and fitting," *Trends Cell Biol.*, vol. 15, pp. 84–91, 2005.

[154] B. L. Sprague *et al.*, "Analysis of binding reactions by fluorescence recovery after photobleaching," *Biophys. J.*, vol. 86, pp. 3473–3495, 2004.

[155] M. A. Medina and P. Schwille, "Fluorescence correlation spectroscopy for the detection and study of single molecules in biology," *Bioessays*, vol. 24, pp. 758–764, 2002.

[156] R. C. Patel *et al.*, "Ligand binding to somatostatin receptors induces receptor-specific oligomer formation in live cells," in *Proc. Nat. Acad. Sci. USA*, vol. 99, pp. 3294–3299, 2002.

[157] A. Amediek *et al.*, "Scanning dual-Color cross-Correlation analysis for dynamic co-Localization studies of immobile molecules," *Single Mol.*, vol. 3, pp. 201–210, 2002.

[158] K. G. Heinze *et al.*, "Two-photon fluorescence coincidence analysis: Rapid measurements of enzyme kinetics," *Biophys. J.*, vol. 83, pp. 1671–1681, 2002.
[159] N. Baudendistel *et al.*, "Two-Hybrid fluorescence cross - Correlation spectroscopy detects protein–Protein interactions in vivo," *ChemPhysChem*, vol. 6, pp. 984–990, 2005.
[160] T. Weidemann *et al.*, "Analysis of ligand binding by two-colour fluorescence cross-correlation spectroscopy," *Single Mol.*, vol. 3, pp. 49–61, 2002.
[161] C. Manzo and M. F. Garcia-Parajo, "A review of progress in single particle tracking: From methods to biophysical insights," *Rep. Progress Phys.*, vol. 78, 2015, Art. no. 124601.
[162] P. M. Carlton *et al.*, "Fast live simultaneous multiwavelength four-dimensional optical microscopy," *Proc. Nat. Acad. Sci. USA*, vol. 107, pp. 16016–16022, 2010.
[163] G. H. Patterson and D. W. Piston, "Photobleaching in two-photon excitation microscopy," *Biophys. J.*, vol. 78, pp. 2159–2162, 2000.
[164] P. Dittrich and P. Schwille, "Photobleaching and stabilization of. fluorophores used for single-molecule analysis. With one-and two-photon excitation," *Appl. Phys. B*, vol. 73, pp. 829–837, 2001.
[165] H. Y. Park *et al.*, "Visualization of dynamics of single endogenous mRNA labeled in live mouse," *Science*, vol. 343, pp. 422–424, 2014.
[166] K. G. Suzuki *et al.*, "Transient GPI-anchored protein homodimers are units for raft organization and function," *Nature Chem. Biol.*, vol. 8, pp. 774–783, 2012.
[167] W. Trabesinger *et al.*, "Detection of individual oligonucleotide pairing by single-molecule microscopy," *Anal. Chem.*, vol. 71, pp. 279–283, 1999.
[168] K. O. Nagata *et al.*, "ABCA1 dimer–monomer interconversion during HDL generation revealed by single-molecule imaging," *Proc. Nat. Acad. Sci. USA*, vol. 110, pp. 5034–5039, 2013.
[169] K. G. Suzuki *et al.*, "GPI-anchored receptor clusters transiently recruit Lyn and Gα for temporary cluster immobilization and Lyn activation: Single-molecule tracking study 1," *J. Cell Biol.*, vol. 177, pp. 717–730, 2007.
[170] S. T. Low-Nam *et al.*, "ErbB1 dimerization is promoted by domain co-confinement and stabilized by ligand binding," *Nature Structural Mol. Biol.*, vol. 18, pp. 1244–1249, 2011.
[171] K. G. Suzuki *et al.*, "Dynamic recruitment of phospholipase Cγ at transiently immobilized GPI-anchored receptor clusters induces IP3–Ca2+ signaling: single-molecule tracking study 2," *J. Cell Biol.*, vol. 177, pp. 731–742, 2007.
[172] H. Murakoshi *et al.*, "Single-molecule imaging analysis of Ras activation in living cells," *Proc. Nat. Acad. Sci. USA*, vol. 101, pp. 7317–7322, 2004.
[173] M. Stracy *et al.*, "Live-cell superresolution microscopy reveals the organization of RNA polymerase in the bacterial nucleoid," *Proc. Nat. Acad. Sci. USA*, vol. 112, pp. E4390–E4399, 2015.
[174] X. Michalet, "Mean square displacement analysis of single-particle trajectories with localization error: Brownian motion in an isotropic medium," *Phys. Rev. E*, vol. 82, 2010, Art no. 041914.
[175] F. L. Groeneweg *et al.*, "Quantitation of glucocorticoid receptor DNA-binding dynamics by single-molecule microscopy and FRAP," *PLoS One*, vol. 9, 2014, Art no. e90532.
[176] S. Semrau and T. Schmidt, "Particle image correlation spectroscopy (PICS): Retrieving nanometer-scale correlations from high-density single-molecule position data," *Biophys. J.*, vol. 92, pp. 613–621, 2007.
[177] I. Chung *et al.*, "Spatial control of EGF receptor activation by reversible dimerization on living cells," *Nature*, vol. 464, pp. 783–787, 2010.
[178] L. Milenkovic *et al.*, "Single-molecule imaging of Hedgehog pathway protein Smoothened in primary cilia reveals binding events regulated by Patched1," *Proc. Nat. Acad. Sci. USA.*, vol. 112, pp. 8320–8325, 2015.
[179] T. Morisaki *et al.*, "Single-molecule analysis of transcription factor binding at transcription sites in live cells," *Nature Commun.*, vol. 5, 2014, Art. no. 4456.
[180] F. Persson *et al.*, "Extracting intracellular diffusive states and transition rates from single-molecule tracking data," *Nature Methods*, vol. 10, pp. 265–269, 2013.
[181] A. Small and S. Stahlheber, "Fluorophore localization algorithms for super-resolution microscopy," *Nature Methods*, vol. 11, pp. 267–279, 2014.
[182] H. Deschout *et al.*, "Precisely and accurately localizing single emitters in fluorescence microscopy," *Nature Methods*, vol. 11, pp. 253–266, 2014.
[183] J. C. Waters, "Accuracy and precision in quantitative fluorescence microscopy," *J. Cell Biol.*, vol. 185, pp. 1135–1148, 2009.
[184] R. P. Nieuwenhuizen *et al.*, "Measuring image resolution in optical nanoscopy," *Nature Methods*, vol. 10, pp. 557–562, 2013.
[185] T. Savin and P. S. Doyle, "Static and dynamic errors in particle tracking microrheology," *Biophys. J.*, vol. 88, pp. 623–638, 2005.
[186] X. S. Xie, "Single-molecule approach to dispersed kinetics and dynamic disorder: Probing conformational fluctuation and enzymatic dynamics," *J. Chem. Phys.*, vol. 117, pp. 11024–11032, 2002.
[187] P. D. Welch, "The use of fast Fourier transform for the estimation of power spectra: A method based on time averaging over short, modified periodograms," *IEEE Trans. Audio Electroacoust.*, vol. AE-15, no. 2, pp. 70–73, Jun. 1967.
[188] R. Roy *et al.*, "A practical guide to single-molecule FRET," *Nature Methods*, vol. 5, pp. 507–516, 2008.

Cong Liu received the B.S. degree in optical engineering from Zhejiang University, Hangzhou, China in 2012. As an undergraduate Research Assistant under the supervision of Prof. Z. Hu, he worked on hemodynamic model-based fMRI BOLD signal analysis. In 2012, he joined Prof. T. Yeh's Group at the University of Texas at Austin as a Ph.D. student in the Biomedical Engineering Department. His graduate research is focused on fluorescence nanomaterials characterization and 3-D single-molecule tracking.

Yen-Liang Liu received the B.S. degree in life science and the M.S. degree in biomedical engineering from National Taiwan University, Taipei, Taiwan. His master's thesis focused on lung tissue engineering and alveolar angiogenesis. The experience as a Tissue Engineer ignited his curiosity to the complex cellular behavior in response to microenvironmental cues. In 2013, he joined Prof. Tim Yeh's Group at the University of Texas at Austin as a Ph.D. student in the Biomedical Engineering Department. Now he applies the single molecule/particle tracking techniques to visualize biomolecule trafficking in live cells.

Evan P. Perillo received the B.S. degree in mechanical engineering from Northeastern University, Boston, MA, USA. He is currently working toward the Ph.D. degree in biomedical engineering at the University of Texas at Austin, TX, USA. His research interests include three-dimensional single particle tracking, *in vivo* two photon microscopy, and ultrafast fiber lasers.

Andrew K. Dunn received the B.S. degree in physics from Bates College, Lewiston, ME, USA, in 1992, the M.S. degree in electrical engineering from Northeastern University, Boston, MA, USA, and the Ph.D. degree in biomedical engineering from University of Texas at Austin. He holds Donald J. Douglass Centennial Professorship in Engineering and Cockrell Family Chair for Departmental Leadership #1 at the University of Texas at Austin. He is also the Director of Center for Emerging Imaging Technologies.

Hsin-Chih Yeh receievd the B.S. degree from National Taiwan University, Taipei, Taiwan, the M.S. degree from the University of California, Los Angeles, CA, USA, and the Ph.D. degree from The Johns Hopkins University, all in mechanical engineering. After graduation from UCLA, he worked at Optical Micro Machines, Inc., in San Diego from 1998 to 2003 as an R&D Engineer, developing MEMS-based photonic switches for telecommunications. He received his postdoctoral training at Los Alamos National Laboratory from 2009 to 2012, in the Center for Integrated Nanotechnologies. He joined the Biomedical Engineering Department, University of Texas at Austin in 2012 as an Assistant Professor. His research interests include nanobiosensor development, 3D molecular tracking and super-resolution imaging.